H. H. Uhlig Corrosion Laboratory
Massachusetts Institute of Technology

LOCALIZED CORROSION INDUCED IN GRAPHITE/ALUMINUM METAL-MATRIX COMPOSITES BY RESIDUAL MICROSTRUCTURAL CHLORIDE

(2)

LOCALIZED CORROSION INDUCED IN
GRAPHITE/ALUMINUM METAL-MATRIX COMPOSITES
BY RESIDUAL MICROSTRUCTURAL CHLORIDE

by

L.H. Hihara and R.M. Latanision

Technical Report
to
Office of Naval Research
Grant No. N00014-89-J-1588

The H.H. Uhlig Corrosion Laboratory
Department of Materials Science and Engineering
Massachusetts Institute of Technology
Cambridge, Massachusetts 02139

February 1990

Unclassified

SECURITY CLASSIFICATION OF THIS PAGE

REPORT DOCUMENTATION PAGE

Form Approved
OMB No. 0704-0188

1a. REPORT SECURITY CLASSIFICATION None

1b. RESTRICTIVE MARKINGS

2a. SECURITY CLASSIFICATION AUTHORITY

2b. DECLASSIFICATION / DOWNGRADING SCHEDULE

3. DISTRIBUTION / AVAILABILITY OF REPORT

4. PERFORMING ORGANIZATION REPORT NUMBER(S)

5. MONITORING ORGANIZATION REPORT NUMBER(S)

6a. NAME OF PERFORMING ORGANIZATION Massachusetts Institute of Technology

6b. OFFICE SYMBOL *(If applicable)*

7a. NAME OF MONITORING ORGANIZATION Office of Naval Research

6c. ADDRESS *(City, State, and ZIP Code)*
Room 8-202, 77 Massachusetts Avenue
Cambridge, MA 02139

7b. ADDRESS *(City, State, and ZIP Code)*
800 N. Quincy Street
Arlington, VA 22217-5000

8a. NAME OF FUNDING / SPONSORING ORGANIZATION Office of Naval Research

8b. OFFICE SYMBOL *(If applicable)*

9. PROCUREMENT INSTRUMENT IDENTIFICATION NUMBER

8c. ADDRESS *(City, State, and ZIP Code)*
Arlington, VA 22217-5000

10. SOURCE OF FUNDING NUMBERS

PROGRAM ELEMENT NO.	PROJECT NO.	TASK NO	WORK UNIT ACCESSION NO.
89-J-1588	cor5523-02		

11. TITLE *(Include Security Classification)*
Localized Corrosion Induced in Graphite/Aluminum Metal-Matrix Composites by Residual Microstructural Chloride

12. PERSONAL AUTHOR(S)
L.H. Hihara and R.M. Latanision

13a. TYPE OF REPORT	13b. TIME COVERED	14. DATE OF REPORT (Year, Month, Day)	15 PAGE COUNT
Technical Report	FROM 1 Mar 89 TO 31Dec89	February 1990	29

16. SUPPLEMENTARY NOTATION

17. COSATI CODES		
FIELD	GROUP	SUB-GROUP

18. SUBJECT TERMS *(Continue on reverse if necessary and identify by block number)*
Corrosion, metal-matrix composites, microstructural chlorides, corrosion kinetics

19. ABSTRACT *(Continue on reverse if necessary and identify by block number)*

Graphite/Al (G/Al) metal-matrix composites (MMCs) manufactured using the titanium-boron vapor deposit (Ti-B VD) method were found susceptible to localized corrosion in chloride-free sodium sulfate solutions in which Al should be passive. Corrosion behavior of G/Al MMC precursor wires and plates made of diffusion-bonded packs of precursor wires was investigated in this study. In chloride-free sodium sulfate solutions, severe pitting of the wire-wire diffusion bonds was observed to coincide with distinct pitting regimes in anodic polarization diagrams of the G/Al MMC plates. The pitting of the diffusion bond regions disbonded the precursor wires, and caused the plates to exfoliate. Pitting was found to be induced by residual microstructural chloride, which originated from the Ti-B VD method. This work suggests that the exfoliation of G/Al MMC plates should be eliminated by producing composites with halide-free microstructures.

20. DISTRIBUTION / AVAILABILITY OF ABSTRACT
☒ UNCLASSIFIED/UNLIMITED ☐ SAME AS RPT. ☐ DTIC USERS

21. ABSTRACT SECURITY CLASSIFICATION Unrestricted

22a. NAME OF RESPONSIBLE INDIVIDUAL	22b. TELEPHONE (Include Area Code)	22c. OFFICE SYMBOL
A.J. Sedriks	(202) 696-4401	1131 M

DD Form 1473, JUN 86 — Previous editions are obsolete. — SECURITY CLASSIFICATION OF THIS PAGE

S/N 0102-LF-014-6603

Localized Corrosion Induced in Graphite/Aluminum Metal-Matrix Composites by Residual Microstructural Chloride

L.H. Hihara* and R.M. Latanision
The H.H. Uhlig Corrosion Laboratory
Department of Materials Science and Engineering
MIT, Cambridge, MA 02139

Abstract

Graphite/Al (G/Al) metal-matrix composites (MMCs) manufactured using the titanium-boron vapor deposit (Ti-B VD) method were found susceptible to localized corrosion in chloride-free sodium sulfate solutions in which Al should be passive. Corrosion behavior of G/Al MMC precursor wires and plates made of diffusion-bonded packs of precursor wires was investigated in this study. In chloride-free sodium sulfate solutions, severe pitting of the wire-wire diffusion bonds was observed to coincide with distinct pitting regimes in anodic polarization diagrams of the G/Al MMC plates. The pitting of the diffusion bond regions disbonded the precursor wires, and caused the plates to exfoliate. Pitting was found to be induced by residual microstructural chloride, which originated from the Ti-B VD method. This work suggests that the exfoliation of G/Al MMC plates should be eliminated by producing composites with halide-free microstructures.

---

* Present address: Department of Mechanical Engineering, University of Hawaii at Manoa, Honolulu, Hawaii 96822

Introduction

Many have speculated [1,2,3,4,5,6] that the poor corrosion resistance of graphite/aluminum (G/Al) metal-matrix composites (MMCs) in comparison to their monolithic matrix alloys is caused by galvanic coupling of graphite and aluminum. However, the exfoliation of composite plates [2,6,7], which are made of diffusion-bonded packs of G/Al MMC precursor wires and Al foils, is more destructive. Exfoliation is caused by the localized corrosion of wire-wire and wire-foil diffusion bonds (DBs), which disbonds precursor wires and foils. The cause of DB corrosion was not determined in the reported cases [2,6,7].

In this study, evidence has been found that correlates localized corrosion of wire-wire DBs and occasional pitting of the matrix to residual chloride, which is left behind in the composite microstructure during fabrication. The Al-infiltration process known as the titanium-boron vapor deposit (Ti-B VD) method of manufacture, which uses $TiCl_4$ (g) and BCl_3 (g) for the deposition of a Ti-B coating on graphite fibers [8], is the source of residual chloride [9]. The microstructure of a graphite/6061-T6 aluminum alloy (G/6061-T6 Al) MMC fabricated by the Ti-B VD method was studied in detail by Hihara and Latanision [9] using Auger electron spectroscopy, x-ray photoelectron spectroscopy, and energy dispersive x-ray analysis (EDXA). The results of Hihara and Latanision [9] will be frequently referenced, and their principal results are summarized below for convenience of the reader. Chloride contamination occurs frequently in the skin of precursor wires and occasionally in fiber-matrix interfaces. Consequently, when precursor wires are diffusion bonded in packs to produce consolidated plates, chloride-containing zones appear in DBs.

The corrosion of G/6061-T6 Al MMCs (processed by the Ti-B VD method) in chloride-free 0.5 M Na_2SO_4 was investigated in this study. Since Al should passivate in chloride-free Na_2SO_4, pitting of the Al-matrix can be attributed to the presence of microstructural chloride. In this study, polarization diagrams were generated for monolithic 6061-T6 Al, graphite fibers, and the MMC. An optical microscope with a video recorder was used with a potentiostat and environmental cell to observe changes occurring on G/6061-T6 Al MMC electrode surfaces in situ. Scanning electron microscopy (SEM) was used to characterize corrosion morphology ex situ. This approach provided 1) electrochemical evidence which demonstrated that pitting of the 6061-T6 Al matrix in chloride-free 0.5 M Na_2SO_4 was induced by microstructural chloride, and 2) visual evidence (in situ and ex situ) of pitting in the DB regions. Correlation between the microstructure, electrochemical data, and corrosion morphology provided firm evidence that links DB corrosion to residual microstructural chloride.

Materials

Monolithic 6061-T6 Al Electrodes:

Planar 6061-T6 Al electrodes were fabricated by coating specimens with either an epoxy paint (AMERCOAT 90 RESIN, Ameron) or an epoxy adhesive (EPOXY-PATCH, The Dexter Corporation). Following the coating procedure, one side of the specimens was ground flat in order to remove the epoxy from one surface to expose a planar electrode face.

P100 Graphite Electrodes:

Planar graphite electrodes were fabricated from Thornel P100 fibers (which are unidirectional, continuous, about 10 μm

in diameter, and pitch-based with an elastic modulus equal to 690 GPa). Fifteen tows of the fiber (≈2000 fibers/tow) were aligned unidirectionally and infiltrated with an epoxy resin (EPON 828 RESIN, Miller-Stephenson Chemical Co., Inc.). The resulting product, a graphite/epoxy composite rod, was made into electrodes by sectioning the rod perpendicularly to the axis of the fibers.

G/6061-T6 Al Electrodes:

G/6061 Al MMC precursor wires were produced by Material Concept, Inc. The wires consisted of a tow of Thornel P100 graphite fibers infiltrated with 6061 Al to a volume fraction of about 0.5. Six-ply plates were consolidated by DWA Composite Specialties, Inc. by diffusion bonding six layers of precursor wires between surface 6061 Al foils. The G/6061 Al MMCs were heat treated to the T6 condition by solution-treating at 530°C for 50 min, water quenching, and artificially aging at 160°C for 18 h.

Planar electrodes were made from G/6061-T6 Al MMC precursor wires and six-ply plates having the graphite fibers oriented perpendicularly to the electrode surface. The surface foils of the six-ply plate were ground away prior to making electrodes. To make electrodes, the specimens were coated with AMERCOAT 90 RESIN and then mounted in EPON 828 RESIN. Following the coating procedure, a planar electrode face was exposed, using the same method described for the 6061-T6 Al electrodes.

Precursor wires were also made into electrodes that exposed only the 6061-T6 Al skin. The tip of the precursor wires was coated with AMERCOAT 90 RESIN to shield the cross section. Consequently, when these precursor wires were

immersed into aqueous solutions, only the 6061-T6 Al skin was exposed. These electrodes will be referred to as precursor-wire 6061-T6 Al skin electrodes.

Aqueous Solutions:

Neutral 0.5 M Na_2SO_4 and 3.15 wt% NaCl solutions were prepared from 18 megaohm-cm water, and analytical grade Na_2SO_4 (< 0.0002% Cl) and NaCl, respectively. During potentiodynamic experiments, the solutions were kept at 30 ± 0.1°C, and deaerated with pre-purified hydrogen or aerated with 19.5 to 23.5 % oxygen balanced with nitrogen. In experiments performed under the optical microscope, solutions were at room temperature and exposed to laboratory air. Gas pressure was 1 atm.

Instrumentation and Procedure

Electrochemical Experimentation

The surface of all planar electrodes was polished to a 0.05 μm finish with gamma alumina powder, kept wet, and rinsed with 18 megaohm-cm water about 5 minutes prior to immersion in the aqueous solutions. The precursor-wire 6061-T6 Al skin electrodes were rinsed in methanol and then in 18 megaohm-cm water about 5 minutes before immersion in the aqueous solutions.

Potentiodynamic polarization examinations were conducted with a Model 173 Princeton Applied Research (PAR) Potentiostat/Galvanostat and a Model 376 PAR Logarithmic Current Converter. The accuracy of the logarithmic current converter was measured to be better than 5% while measuring currents in the nA range.

In generating potentiodynamic polarization diagrams, the electrodes were allowed to stabilize at their corrosion potentials (E_{corr}) and were subsequently polarized at a rate of 0.1 mV/s. Polarization diagrams with error bars were generated from at least three individual polarization diagrams. The average logarithm of the current density (log i [A/cm^2]) was plotted as a function of potential. The peak-to-peak width between error bars is equal to two times the standard deviation of log i. The average values of E_{corr}, the average time that the electrodes were in the open circuit condition prior to polarization, and the standard deviation (SD) of these parameters are given in the caption of the polarization diagrams.

Corrosion Morphology

Optical microscopy and SEM were used to characterize the corrosion morphology. Chemical analysis of solid corrosion products was performed by EDXA.

In situ corrosion observations were made using an optical microscope equipped with a video camera and recorder. An open cell contained the solution and held the specimen beneath the objective lens of the microscope. There were several millimeters of solution above the specimen surface.

Results

Electrochemical Data

In order to recognize peculiarities in the electrochemical behavior of the G/6061-T6 Al MMC plate (exposed to 0.5 M Na_2SO_4), the anodic polarization diagram of the actual composite was compared to that of a multiple electrode model.

The model represented "ideal" behavior. Accordingly, anodic polarization diagrams of monolithic 6061-T6 Al, P100 graphite fiber, and G/6061-T6 Al MMCs were generated. Because residual microstructural chloride is expected to induce pitting in the 6061-T6 Al matrix, it is important to know how chloride affects the anodic polarization diagram of 6061-T6 Al. For this reason, an anodic polarization diagram of monolithic 6061-T6 Al exposed to 3.15 wt% NaCl was generated.

Monolithic 6061-T6 Al:

Anodic polarization diagrams of 6061-T6 Al are shown in Figures 1 (deaerated 0.5 M Na_2SO_4) and 2 (deaerated 3.15 wt% NaCl). The 6061-T6 Al passivated in the Na_2SO_4 solution, and pitted in the NaCl solution (pitting potential ≈ -0.725 V_{SCE}).

P100 Graphite Fiber:

The anodic polarization diagram of P100 graphite fiber exposed to deaerated 0.5 M Na_2SO_4 is shown in Figure 1.

G/6061-T6 Al MMC:

Anodic polarization diagrams of planar six-ply plate (Figures 3) and precursor wire (Figure 4) that were exposed to deaerated 0.5 M Na_2SO_4 are similar, with pitting potentials at approximately -0.5 V_{SCE}. The open circuit potential of planar six-ply plate electrodes was shifted in the noble direction towards the pitting potential during aeration, as shown in Figure 5. The anodic polarization diagram of the precursor-wire 6061-T6 Al skin electrode (Figure 6) exposed to deaerated 0.5 M Na_2SO_4 is also similar to Figures 3 and 4; the pitting potential of the precursor-wire skin was about -0.6 V_{SCE}.

Corrosion Morphology

In chloride-free 0.5 M Na_2SO_4, the matrix of the G/6061-T6 Al MMC pitted in the zones of residual microstructural chloride. Of the various types of electrodes examined, the zones were located in 1) the DB regions of the planar six-ply plate electrodes, 2) the perimeter regions of the planar precursor w. . electrodes, and 3) the skin of the precursor-wire 6061-T6 Al skin electrodes. The graphite fibers were relatively inert, but could be oxidized at noble potentials.

Planar Six-ply Plate Electrodes:

The corrosion process was observed in situ with an optical microscope, and can be viewed on video tape elsewhere [10]. Hydrogen evolution was observed in the DB regions during exposure to aerated 0.5 M Na_2SO_4 in the open circuit condition (-0.61 V_{SCE}). Dissolution of the DB regions was intensified by anodic polarization, and the resulting corrosion morphology is shown in Figure 7. The disbonding of precursor wires by corrosion was demonstrated by sawing off the surface layer from a corroded electrode, similar to that in Figure 7, to produce a wafer which could then be slightly stressed in tension. Following this procedure, the wafer parted along thoroughly-corroded DBs (Figure 8); the corrosion product in the region contained chlorine, as determined by EDXA. Occasionally, pits were also found in precursor interiors, as shown in Figure 9.

Planar Precursor Wire Electrodes:

Pits were concentrated near the perimeter of planar precursor-wire electrodes (Figure 10) that were anodically polarized in 0.5 M Na_2SO_4. With the optical microscope, H_2 evolution was also seen in the perimeter regions during

anodic polarization (at 0.0 V_{SCE}). In this case, H_2 evolution is an indication of pitting because the reducing potentials within pits can promote H_2 evolution.

Precursor-wire 6061-T6 Al Skin Electrodes:

Pits were copious in the skin of precursor-wire 6061-T6 Al skin electrodes (Figure 11) that were anodically polarized in deaerated 0.5 M Na_2SO_4. Beneath the skin, dissolution of the matrix was extensive, as shown by a cross-sectional slice (Figure 12). An enlargement of the cross section shows sites where pits penetrated the skin (Figure 13). In Figures 12 and 13, the large cavities (black) resulted from mechanical damage during sectioning.

Graphite Fiber in G/6061-T6 Al MMC:

Figure 14 shows crevices that formed along perimeters of graphite fibers during anodic polarization at 2.0 V_{SCE} for 3.2 hours at 30°C in deaerated 0.5 M Na_2SO_4.

Discussion

The electrochemical evidence of pitting in chloride-free 0.5 M Na_2SO_4, and the localized corrosion of DB regions are two principal findings presented in the Results section. These results in concert with those of Hihara and Latanision [9], which revealed that chloride-containing zones are located in DB regions, provide sufficient evidence to link DB corrosion to residual microstructural chloride. The following discussion establishes that 1) pitting was induced by residual chloride, as revealed by a comparison of the electrochemical behavior of the multiple electrode model to that of the actual MMC, 2) corrosion morphology was related to the microstructure, 3) DB corrosion in the open circuit condition was caused by O_2 reduction, and

4) crevice formation, which occurs along the perimeters of P100 graphite fibers, was caused by graphite oxidation and not by fiber-matrix interfacial dissolution.

The multiple electrode model for a composite containing 50% P100 graphite fibers and 6061-T6 Al exposed to deaerated 0.5 M Na_2SO_4 is shown in Figure 1. In the multiple electrode model, 6061-T6 Al was passive, and P100 graphite was oxidized primarily to CO_2. Hihara [10] showed that significant amounts of CO_2 are liberated from P100 graphite anodes during polarization in 0.5 M Na_2SO_4. In Figure 15, the polarization diagram of the multiple electrode model is compared to the actual diagram of the G/6061-T6 Al MMC six-ply plate. The pitting regime in the polarization diagram of the six-ply plate (Figure 3 or 15) caused current densities to be much larger than predicted by the multiple electrode model. In fact, pitting regimes were found in all of the anodic polarization diagrams of the various G/6061-T6 Al electrodes exposed to chloride-free 0.5 M Na_2SO_4. This can be seen in Figures 4 and 6, showing the anodic polarization diagrams of the planar precursor wire and precursor-wire 6061-T6 Al skin electrodes, respectively. It is evident that microstructural chloride induces pitting of 6061-T6 Al in much the same manner as would Cl^- ions originating from solution. This was further demonstrated by comparing the anodic polarization diagram of the precursor-wire 6061-T6 Al skin electrode exposed to chloride-free 0.5 M Na_2SO_4 to that of monolithic 6061-T6 Al exposed to 3.15 wt% NaCl (Figure 16). Although there is a difference in the pitting potentials by about 0.1 V (Figure 16), the difference was anticipated due to the dependency of pitting potentials on chloride-ion concentration [11].

The corrosion morphology also provided firm evidence that links localized corrosion to microstructural chloride. High pit density corresponded to the zones of microstructural chloride. In the planar electrodes, the zones were located in the DB regions of six-ply plates, and in the perimeter of precursor wires. In the precursor-wire 6061-T6 Al skin electrodes, the zone encompassed the skin [9]. Accordingly, in the planar electrodes, severe pitting occurred in the DB regions of six-ply plates (Figures 7 and 8) and in the perimeter regions of precursor wires (Figure 10). In the precursor-wire skin electrode, the skin severely pitted (Figures 11, 12, and 13). Also, the corrosion of DB regions led to the disbonding of precursor wires in the six-ply plate electrodes. It is likely that this type of disbonding resulted in the exfoliation of G/Al plates that were seen by others [2,6,7]. An important implication is that composites with halide-free DBs should not exfoliate.

In the six-ply plates, pitting of the matrix also occurred in precursor-wire interiors, as shown in Figure 9. Pitting in the precursor interiors, which occurred infrequently in comparison to pitting in the DB regions, is probably induced by chloride contamination of fiber-matrix interfaces, which is also infrequent [9].

It is also important to know if pitting occurs in the open circuit condition, which is likely to be the case during service conditions. In deaerated 0.5 M Na_2SO_4, the polarization diagrams (Figures 3, 4, and 6) show that G/6061-T6 Al MMCs were spontaneously passive. In aerated solutions, however, a planar six-ply plate electrode (exposed to 0.5 M Na_2SO_4) was polarized into the vicinity of the pitting regime by O_2 reduction. This is shown in Figure 5 where the open circuit potential

approaches the pitting potential. Hydrogen evolution was also observed (in situ with an optical microscope) in the DB regions of newly polished six-ply plate exposed to aerated 0.5 M Na_2SO_4 in the open circuit condition (-0.61 V_{SCE}). H_2 evolution, in this case, is a sign of pitting because potentials within pits can be sufficiently reducing to promote H_2 evolution. It is doubtful that methane evolution resulting from Al_4C_3 hydrolysis or graphite reduction can occur at DB regions. Al_4C_3 should be localized in fiber-matrix interfaces and not in DBs because it is a reaction product of graphite and Al at high processing temperatures. Methane, which is thermodynamically stable at cathodic potentials, was undetectable during cathodic polarization of P100 graphite fiber electrodes in 0.5 M Na_2SO_4 [10].

Finally, comments are due regarding crevices that formed along fiber perimeters (Figure 14) which could be mistaken for dissolution of fiber-matrix interfaces. The crevices formed during anodic polarization in 0.5 M Na_2SO_4. The corrosion morphology shown in Figure 14 is identical to that seen in graphite/epoxy composites [10]. Epoxy is unaffected by anodic polarization whereas the graphite fibers are oxidized primarily to CO_2 [10]. Since the Al matrix in G/6061-T6 Al MMCs should passivate near fiber-matrix interfaces (where microstructural chloride is rarely found [9]), the corrosion morphology is expected to be similar to that of graphite/epoxy composites. Thus, the apparent interfacial dissolution was actually the result of graphite oxidation.

Conclusion

Chloride-containing zones in DBs of G/6061-T6 Al MMC plates were found to cause severe pitting in DB regions. The pitting of DB regions disbonds precursor wires, which leads to

the exfoliation of six-ply plate electrodes. Exfoliation is much more destructive than classical galvanic corrosion between graphite and Al. This work suggests that exfoliation can be eliminated from future G/Al MMCs by producing composites with halide-free DBs. In view of these findings, priority should be given to fabrication processes that do not use halides.

Acknowledgements

We are grateful for the financial support provided by the Shell Companies Foundation and the Office of Naval Research (grant # N00014-89-J-1588). We are particularly grateful to Dr. S.G. Fishman of the Office of Naval Research, and to Dr. W.C. Harrigan, Jr. of DWA Composite Specialties, Inc.

References

1) W.F. Czyrklis, Corrosion/85, Paper No. 196, NACE, Houston, Texas, 1985.

2) M.G. Vassilaros, D.A. Davis, G.L. Steckel, J.P. Gudas, in Mechanical Behavior of Metal-Matrix Composites, Ed. J.E. Hack, M.F. Amateau, The Metallurgical Society of the AIME, 1983, p.335.

3) D.L. Dull, W.C. Harrigan, Jr., M.F. Amateau, Aerospace Corporation, AD - A011 761, 1975.

4) J.M. Evans, D.M. Braddick, Corros. Sci., Vol.11, 1971, p.611.

5) E.G. Kendall, D.L. Dull, "Salt Water Corrosion Behavior of Aluminum-Graphite Composite," National Technical Information Service, U.S. Department of Commerce, AD-777 160, 1974.

6) D.M. Aylor, R.M. Kain, in Recent Advances in Composites in the United States and Japan, Ed. J.R. Vinson, M. Taya, ASTM Special Technical Publication 864, 1983, p.632.

7) W.H. Pfeifer, in Hybrid and Select Metal-Matrix Composites, Ed. W.J. Renton, American Institute of Aeronautics and Astronautics, 1977, p.231.

8) W.C. Harrigan, Jr., R.H. Flowers, in Failure Modes in Composites IV, Ed. J.A. Cornie, F.W. Crossman, The Metallurgical Society of AIME, 1977, p.319.

9) L.H. Hihara, R.M. Latanision, Mater. Sci. E. A, in Press.

10) L.H. Hihara, "Corrosion of Aluminum-Matrix Composites," Ph.D. Thesis, Massachusetts Institute of Technology, 1989.

11) J.R. Galvele, in Passivity of Metals, Ed. R.P. Frankenthal, J. Kruger, The Electrochemical Society, Inc. 1978, p.285.

List of Figures

Figure 3: Anodic polarization diagram of planar G/6061-T6 Al MMC six-ply plate electrode exposed to deaerated 0.5 M Na_2SO_4 of pH 7 at 30°C. Scan rate = 0.1 mV/s; Avg E_{CORR} = -0.915 V_{SCE}, SD = 0.018 V; Avg time at open circuit = 0.93 h, SD = 0.17 h.

Figure 4: Anodic polarization diagram of planar G/6061-T6 Al MMC precursor wire electrode exposed to deaerated 0.5 M Na_2SO_4 of pH 7 at 30°C. Scan rate = 0.1 mV/s; Avg E_{CORR} = -1.050 V_{SCE}, SD = 0.005 V; Avg time at open circuit = 0.62 h, SD = 0.03 h.

Figure 5: Anodic polarization diagram of planar G/6061-T6 Al MMC six-ply plate electrode exposed to aerated 0.5 M Na_2SO_4 of pH 7 at 30°C. Scan rate = 0.1 mV/s; Avg E_{CORR} = -0.680 V_{SCE}, SD = 0.048 V; Avg time at open circuit = 1.55 h, SD = 0.57 h.

Figure 6: Anodic polarization diagram of precursor-wire 6061-T6 Al skin electrode exposed to deaerated 0.5 M Na_2SO_4 of pH 7 at 30°C. Scan rate = 0.1 mV/s; Avg E_{CORR} = -1.081 V_{SCE}, SD = 0.017 V; Avg time at open circuit = 0.71 h, SD = 0.08 h.

Figure 7: SEM micrograph showing the localized dissolution (induced by residual microstructural chloride) of the diffusion bond regions between precursor wires in a planar G/6061-T6 Al MMC six-ply plate electrode. The electrode was anodically polarized in deaerated 0.5 M Na_2SO_4 of pH 7 at 30°C.

Figure 8: SEM micrograph of a planar G/6061-T6 Al MMC six-ply plate electrode showing the disbonding of precursor wires resulting from localized dissolution (induced by residual microstructural chloride) of the diffusion bond regions. The electrode was anodically polarized in deaerated 0.5 M Na_2SO_4 of pH 7 at 30°C.

Figure 9: SEM micrograph of a planar G/6061-T6 Al MMC six-ply plate electrode showing localized dissolution (induced by residual microstructural chloride) in precursor interiors. Graphite fibers (dark) are in a 6061-T6 Al matrix (light). The electrode was anodically polarized in deaerated 0.5 M Na_2SO_4 of pH 7 at 30°C.

Figure 10: SEM micrograph showing localized dissolution (induced by residual microstructural chloride) in the perimeter region (indicated by arrows) of a planar G/6061-T6 Al MMC precursor wire electrode. The graphite fibers (dark) are in a 6061-T6 Al matrix (light). The precursor wire is mounted in epoxy. The electrode was anodically polarized in deaerated 0.5 M Na_2SO_4 of pH 7 at 30°C.

Figure 11: SEM micrograph showing pits (induced by residual microstructural chloride) in a precursor-wire skin electrode. The electrode was anodically polarized in deaerated 0.5 M Na_2SO_4 of pH 7 at 30°C.

Figure 12: Cross section of the precursor-wire 6061-T6 Al skin electrode shown in Figure 11. The graphite fibers (dots) are perpendicular to the plane of the page. The bright regions are unconsumed 6061-T6 Al matrix. The electrode was anodically polarized in deaerated 0.5 M Na_2SO_4 of pH 7 at 30°C.

Figure 13: Enlarged view of Figure 12 showing sites where pits (indicated by arrows) initially penetrated the precursor-wire skin.

Figure 14: SEM micrograph showing crevices along the perimeters of graphite fibers in a planar G/6061-T6 Al MMC six-ply plate electrode that was anodically polarized at 2.0 V_{SCE} for 3.2 h in deaerated 0.5 M Na_2SO_4 of pH 7 at 30°C. The formation of crevices was caused by CO_2 evolution, resulting from the oxidation of graphite.

Figure 15: Comparison of the anodic polarization diagram of the multiple electrode model (consisting of 50% P100 graphite fiber and 6061-T6 Al) to that of the planar G/6061-T6 Al MMC (≈50 vol % P100 graphite) six-ply plate electrode exposed to deaerated 0.5 M Na_2SO_4 of pH 7 at 30°C. Scan rate = 0.1 mV/s.

Figure 16: Comparison of the anodic polarization diagram of the precursor-wire 6061-T6 Al skin electrode exposed to deaerated chloride-free 0.5 M Na_2SO_4 to that of monolithic 6061-T6 Al exposed to deaerated 3.15 wt% NaCl. Both solutions were of pH 7 at 30°C. Scan rate = 0.1 mV/s.

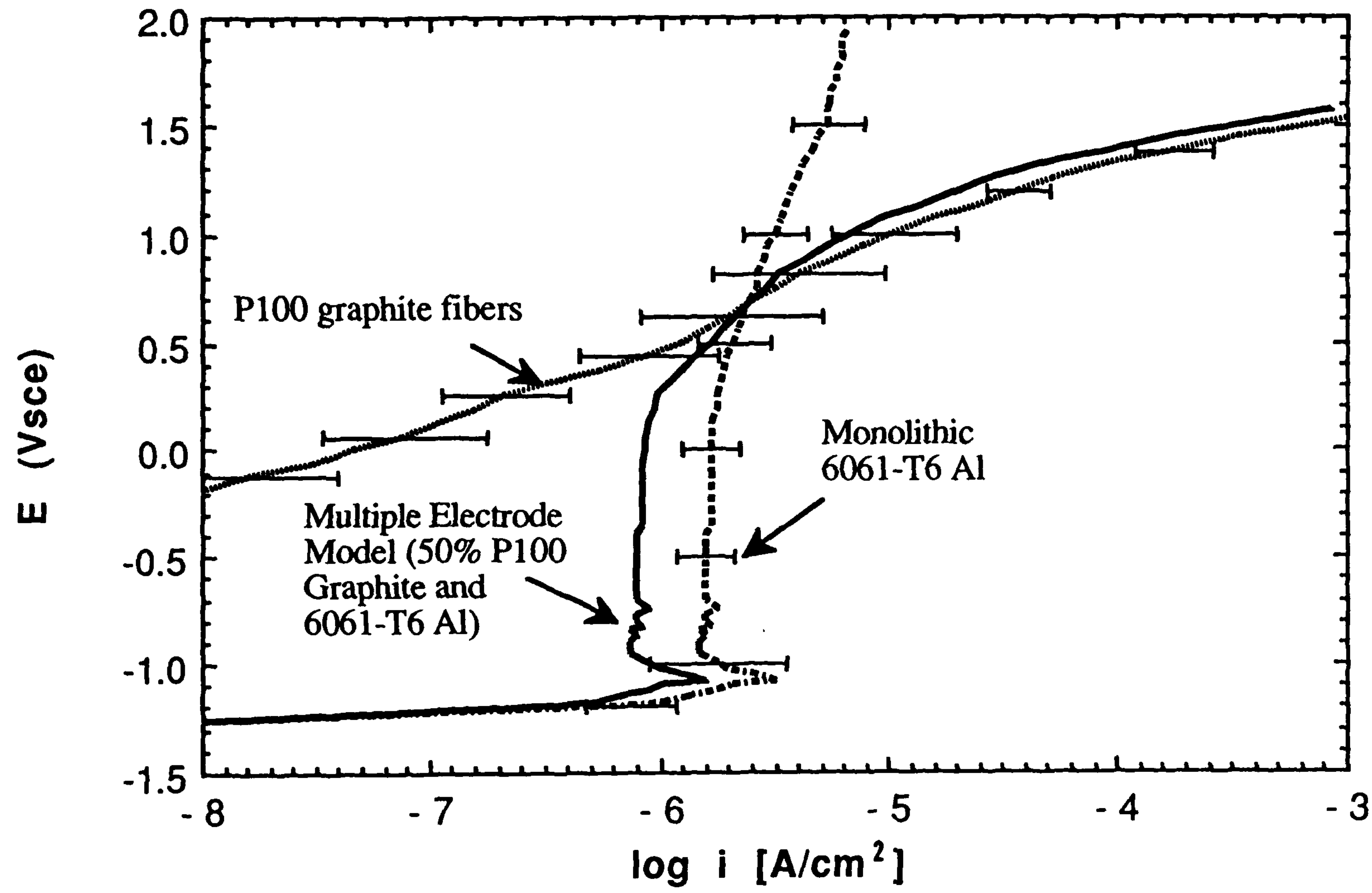

Figure 1: Anodic polarization diagrams of 6061-T6 Al and P100 graphite fiber exposed to deaerated 0.5 M Na_2SO_4 of pH 7 at 30°C. Scan rate = 0.1 mV/s. Based on the mixed electrode theory, these diagrams were used to construct the anodic polarization diagram of a composite consisting of 50% P100 graphite fiber and 6061-T6 Al. Data for 6061-T6 Al: Avg E_{CORR} = -1.256 V_{SCE}, SD = 0.010 V; Avg time at open circuit = 0.59 h, SD = 0.09 h. Data for P100 graphite fiber: Avg E_{CORR} = -0.190 V_{SCE}, SD = 0.64 V; Avg time at open circuit = 2.21 h, SD = 1.11 h.

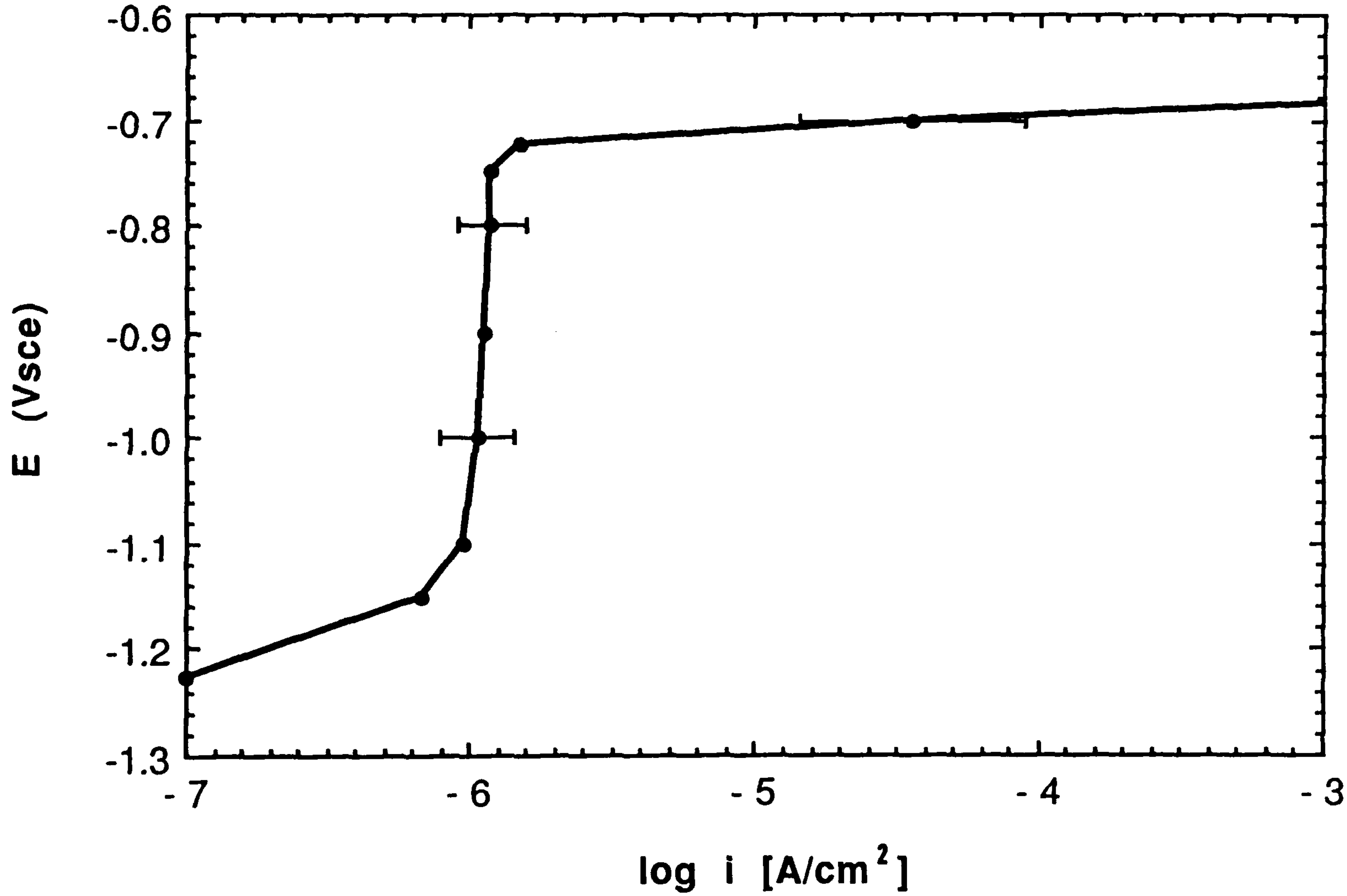

Figure 2: Anodic polarization diagram of 6061-T6 Al exposed to deaerated 3.15 *wt%* NaCl of pH 7 at 30°C. Scan rate = 0.1 mV/s; Avg E_{CORR} = -1.228 V_{SCE}, SD = 0.029 V; Avg time at open circuit = 0.67 h, SD = 0.18 h.

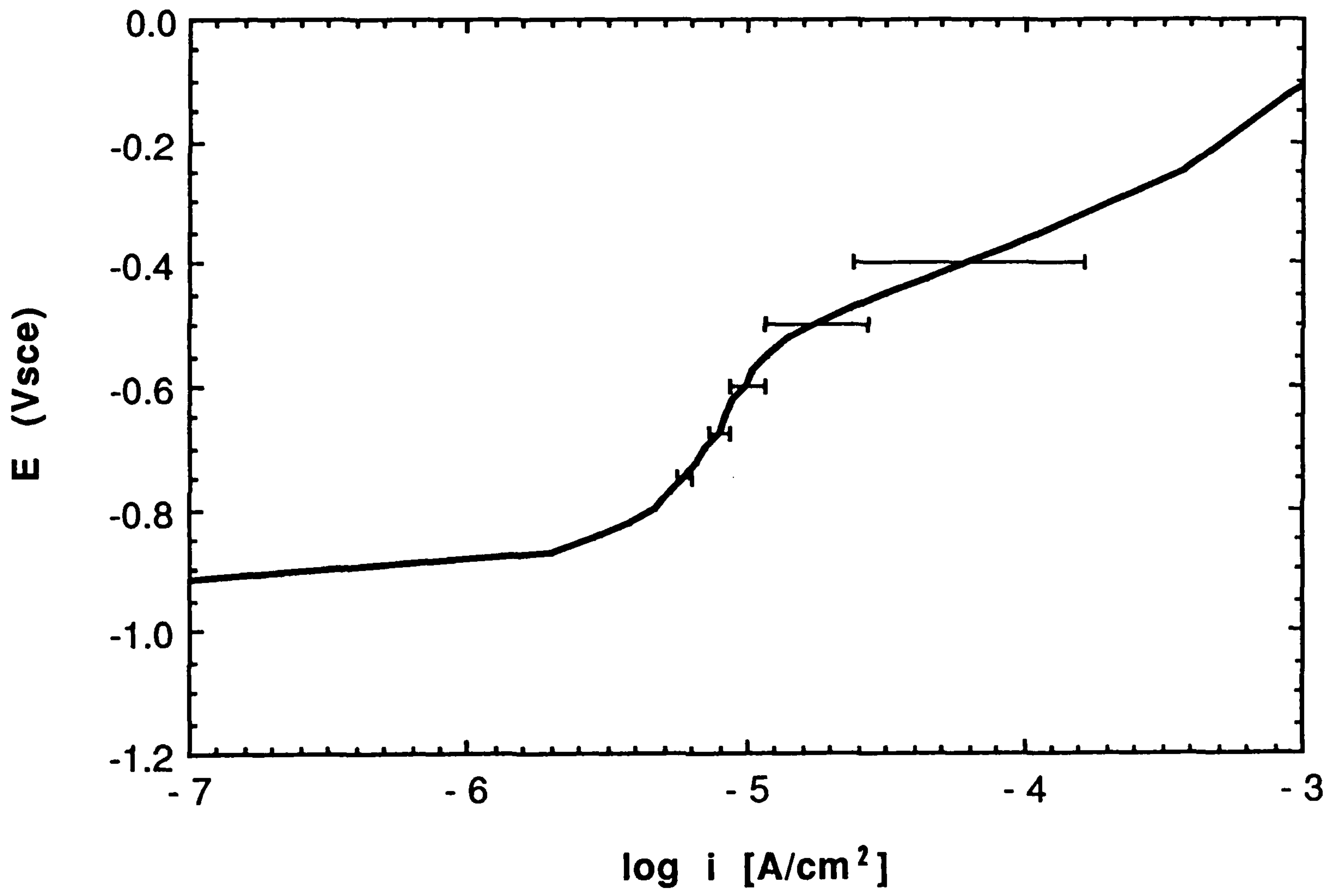

Figure 3: Anodic polarization diagram of planar G/6061-T6 Al MMC six-ply plate electrode exposed to deaerated 0.5 M Na_2SO_4 of pH 7 at 30°C. Scan rate = 0.1 mV/s; Avg E_{CORR} = -0.915 V_{SCE}, SD = 0.018 V; Avg time at open circuit = 0.93 h, SD = 0.17 h.

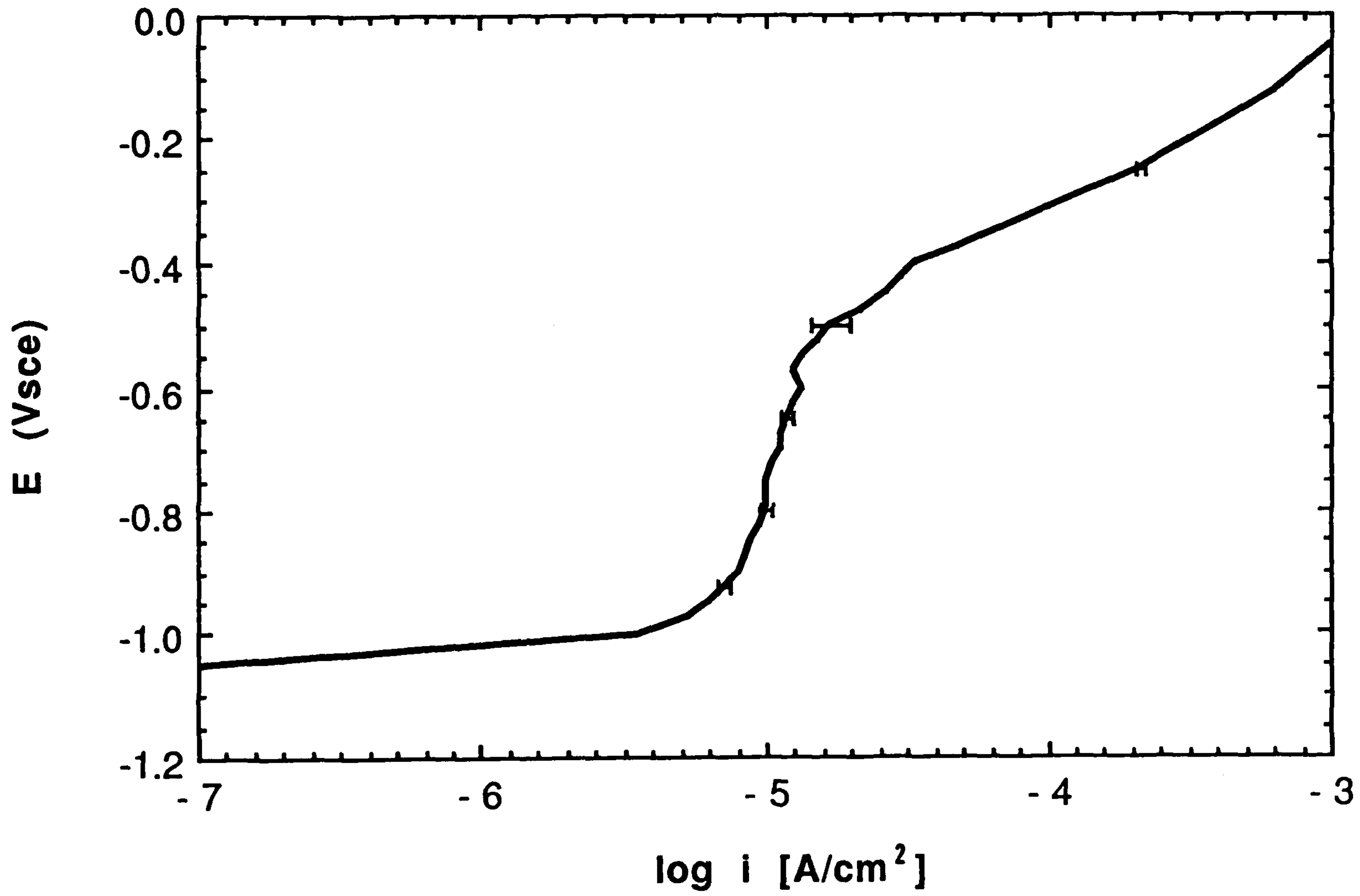

Figure 4: Anodic polarization diagram of planar G/6061-T6 Al MMC precursor wire electrode exposed to deaerated 0.5 M Na_2SO_4 of pH 7 at 30°C. Scan rate = 0.1 mV/s; Avg E_{CORR} = -1.050 V_{SCE}, SD = 0.005 V; Avg time at open circuit = 0.62 h, SD = 0.03 h.

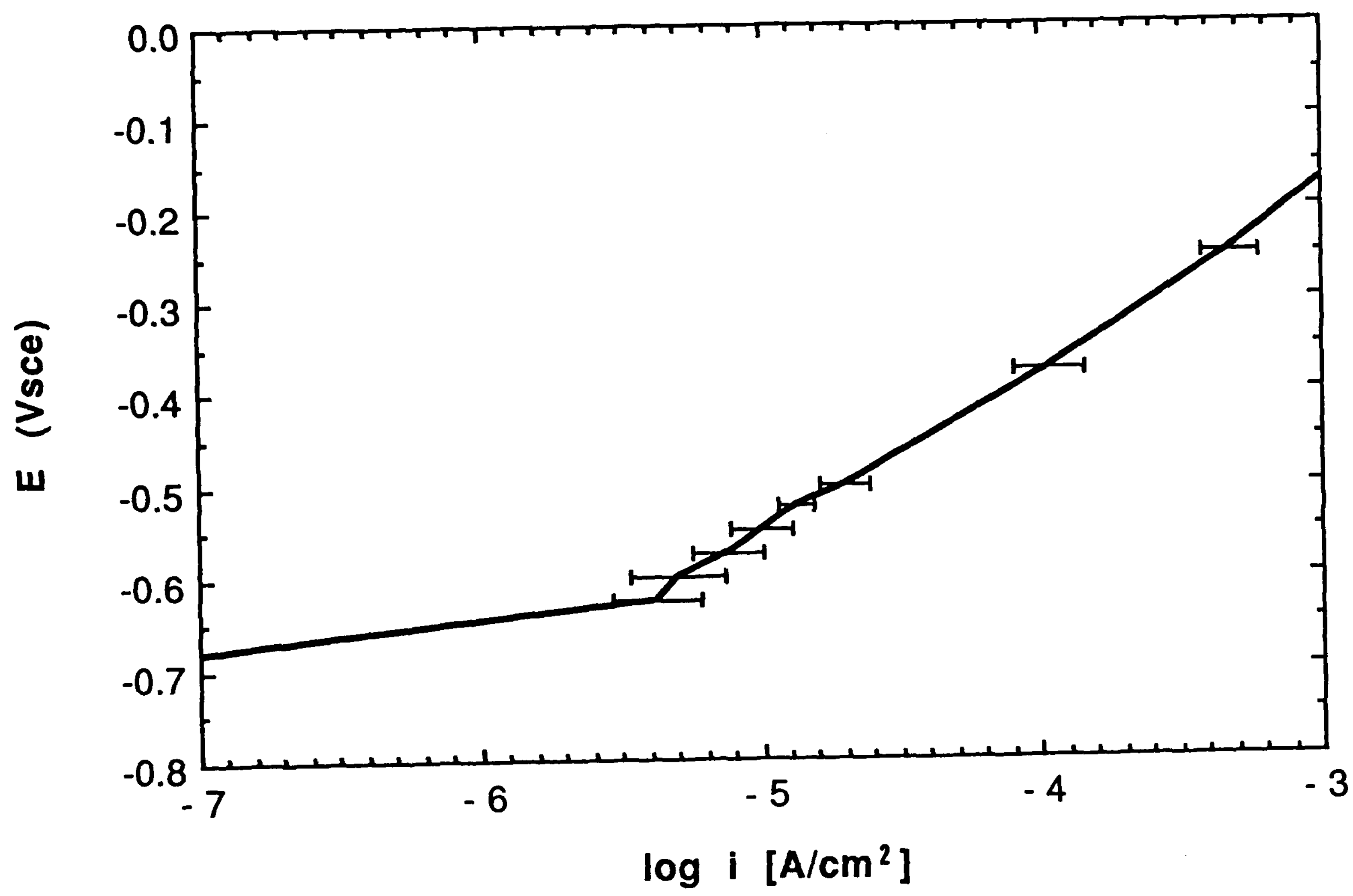

Figure 5: Anodic polarization diagram of planar G/6061-T6 Al MMC six-ply plate electrode exposed to aerated 0.5 M Na_2SO_4 of pH 7 at 30°C. Scan rate = 0.1 mV/s; Avg E_{CORR} = -0.680 V_{SCE}, SD = 0.048 V; Avg time at open circuit = 1.55 h, SD = 0.57 h.

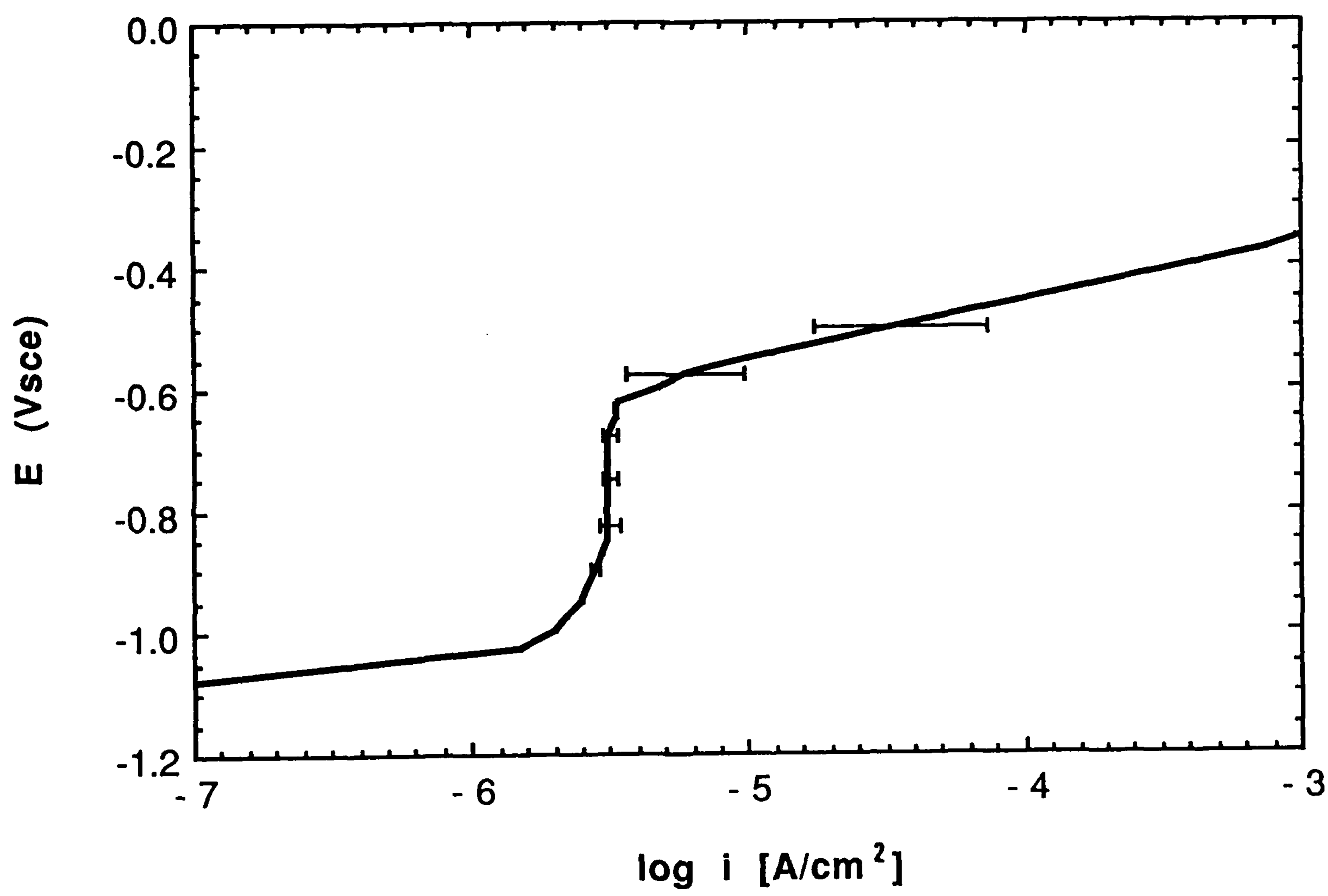

Figure 6: Anodic polarization diagram of precursor-wire 6061-T6 Al skin electrode exposed to deaerated 0.5 M Na_2SO_4 of pH 7 at 30°C. Scan rate = 0.1 mV/s; Avg E_{CORR} = -1.081 V_{SCE}, SD = 0.017 V; Avg time at open circuit = 0.71 h, SD = 0.08 h.

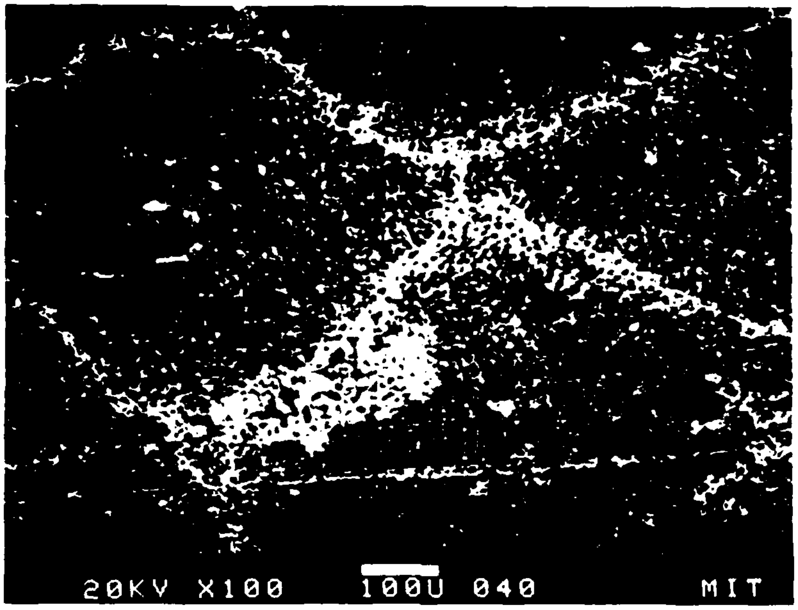

Figure 7: SEM micrograph showing the localized dissolution (induced by residual microstructural chloride) of the diffusion bond regions between precursor wires in a planar G/6061-T6 Al MMC six-ply plate electrode. The electrode was anodically polarized in deaerated 0.5 M Na_2SO_4 of pH 7 at 30°C.

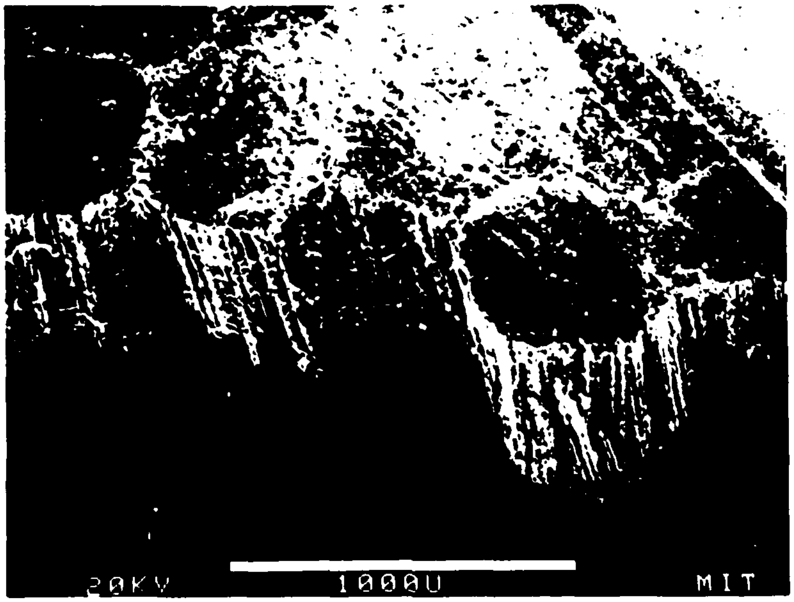

Figure 8: SEM micrograph of a planar G/6061-T6 Al MMC six-ply plate electrode showing the unbinding of precursor wires resulting from localized dissolution (induced by residual microstructural chloride) of the diffusion bond regions. The electrode was anodically polarized in deaerated 0.5 M Na_2SO_4 of pH 7 at 30°C.

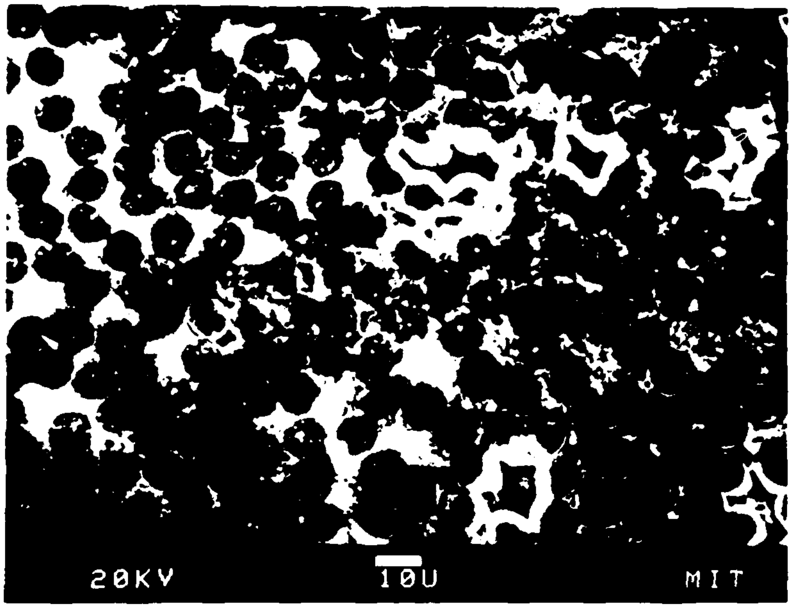

Figure 9: SEM micrograph of a planar G/6061-T6 Al MMC six-ply plate electrode showing localized dissolution (induced by residual microstructural chloride) in precursor interiors. Graphite fibers (dark) are in a 6061-T6 Al matrix (light). The electrode was anodically polarized in deaerated 0.5 M Na_2SO_4 of pH 7 at 30°C.

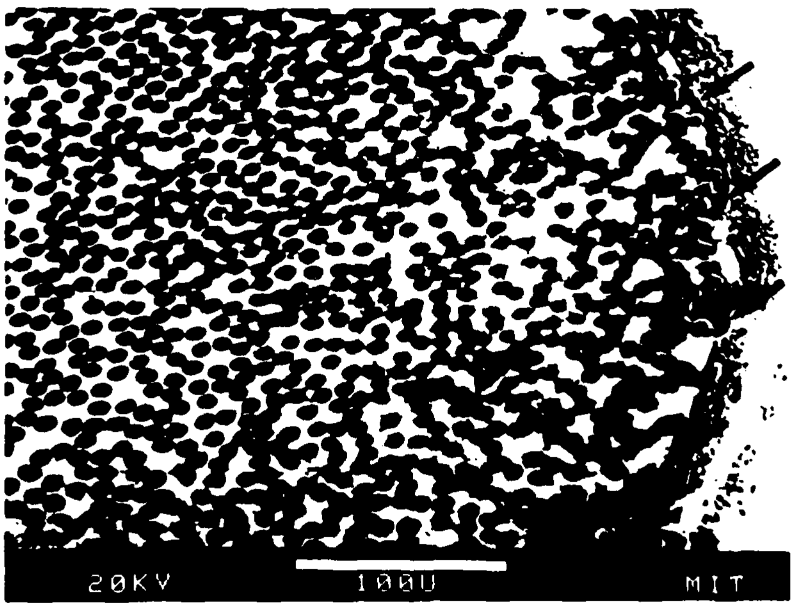

Figure 10: SEM micrograph showing localized dissolution (induced by residual microstructural chloride) in the perimeter region (indicated by arrows) of a planar G/6061-T6 Al MMC precursor wire electrode. The graphite fibers (dark) are in a 6061-T6 Al matrix (light). The precursor wire is mounted in epoxy. The electrode was anodically polarized in deaerated 0.5 M Na_2SO_4 of pH 7 at 30°C.

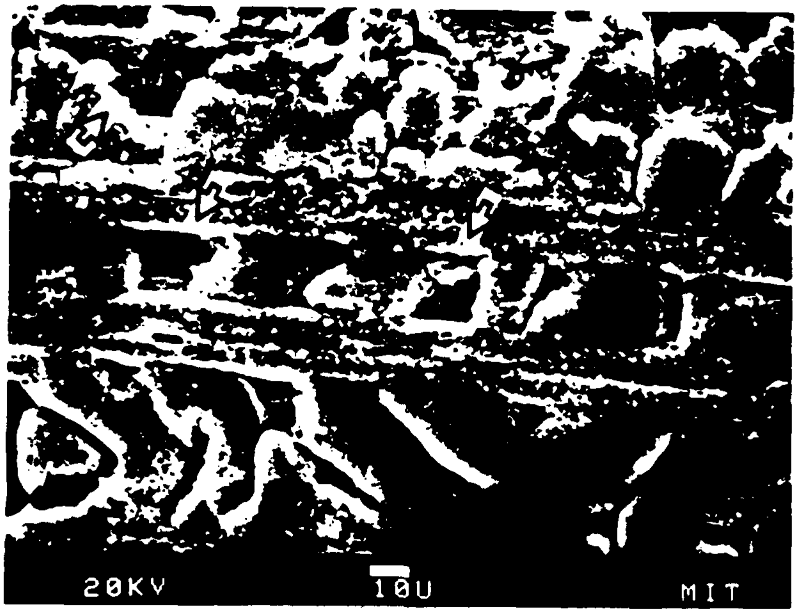

Figure 11: SEM micrograph showing pits (induced by residual microstructural chloride) in a precursor-wire skin electrode. The electrode was anodically polarized in deaerated 0.5 M Na_2SO_4 of pH 7 at 30°C.

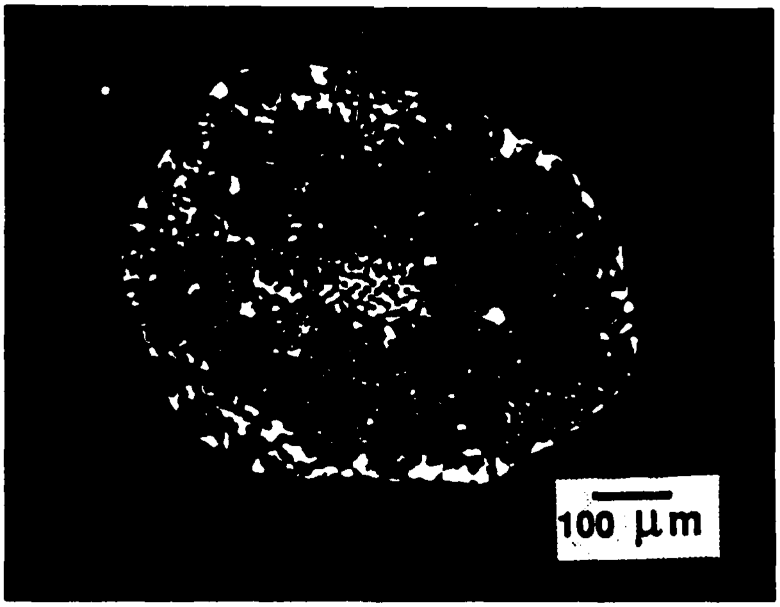

Figure 12: Cross section of the precursor-wire 6061-T6 Al skin electrode shown in Figure 11. The graphite fibers (dots) are perpendicular to the plane of the page. The bright regions are unconsumed 6061-T6 Al matrix. The electrode was anodically polarized in deaerated 0.5 M Na_2SO_4 of pH 7 at 30°C.

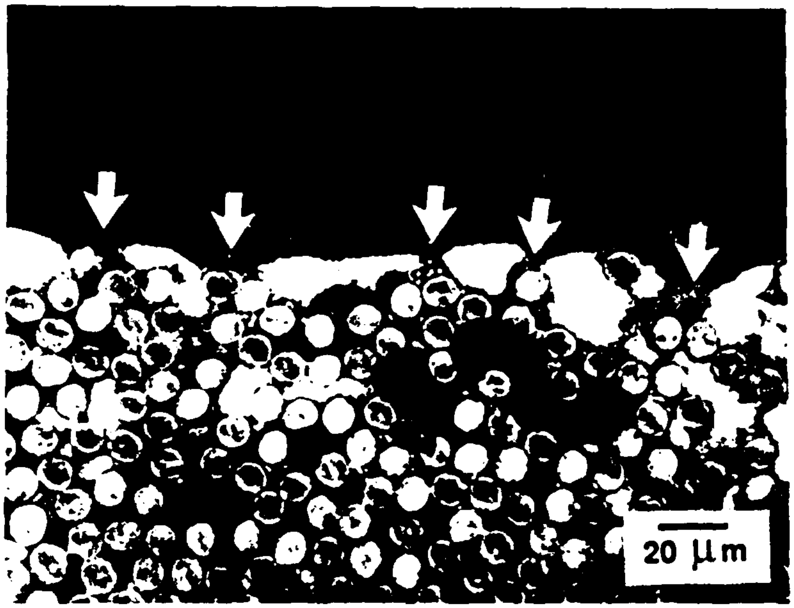

Figure 13: Enlarged view of Figure 12 showing sites where pits (indicated by arrows) initially penetrated the precursor-wire skin.

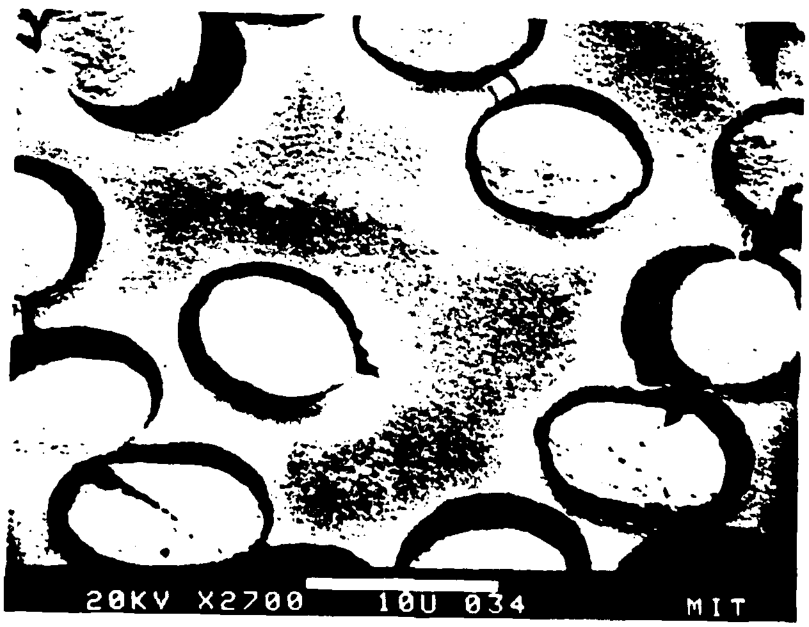

Figure 14: SEM micrograph showing crevices along the perimeters of graphite fibers in a planar G/6061-T6 Al MMC six-ply plate electrode that was anodically polarized at 2.0 V_{SCE} for 3.2 h in deaerated 0.5 M Na_2SO_4 of pH 7 at 30°C. The formation of crevices was caused by CO_2 evolution, resulting from the oxidation of graphite.

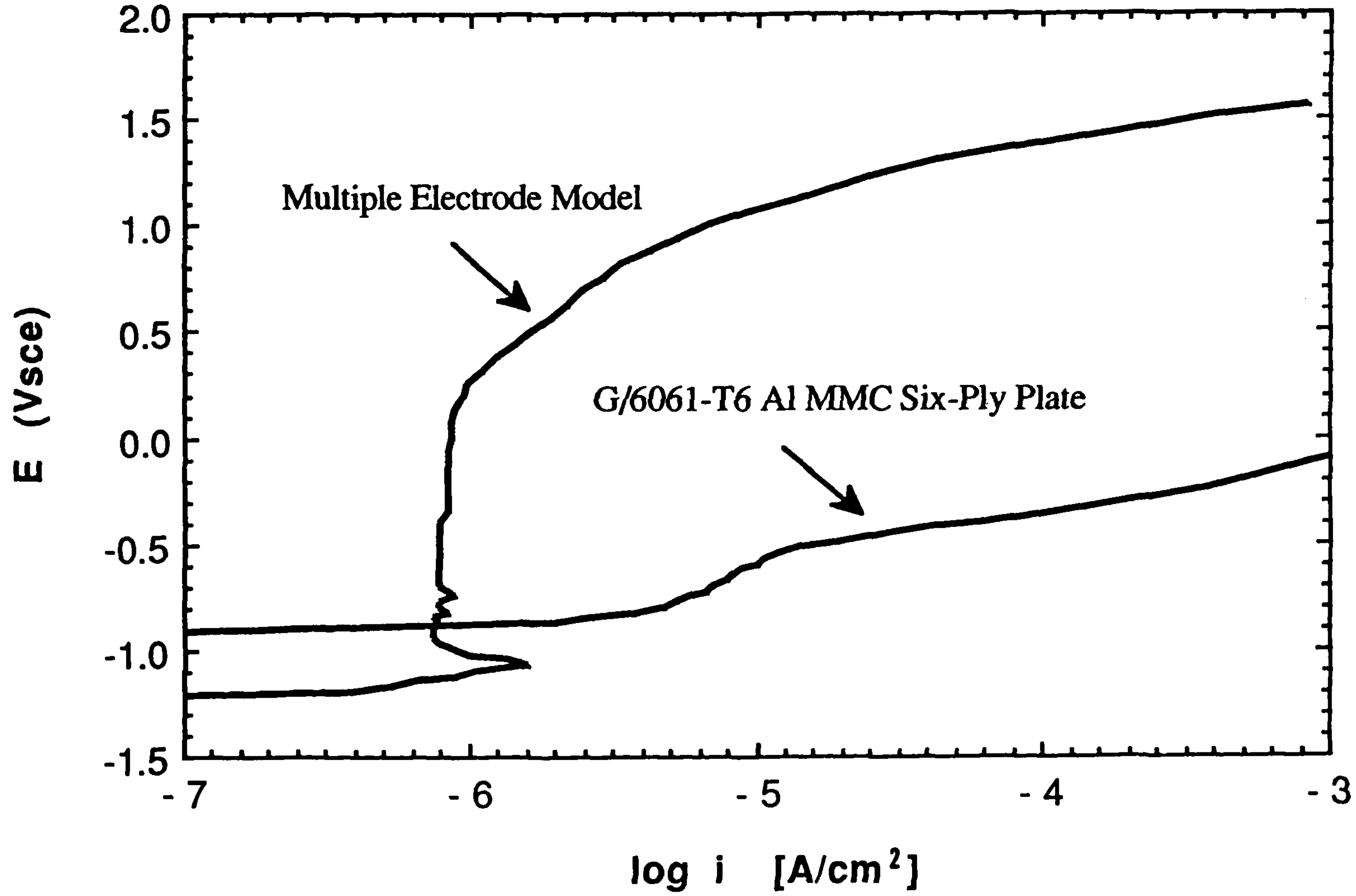

Figure 15: Comparison of the anodic polarization diagram of the multiple electrode model (consisting of 50% P100 graphite fiber and 6061-T6 Al) to that of the planar G/6061-T6 Al MMC (≈50 vol % P100 graphite) six-ply plate electrode exposed to deaerated 0.5 M Na_2SO_4 of pH 7 at 30°C. Scan rate = 0.1 mV/s.

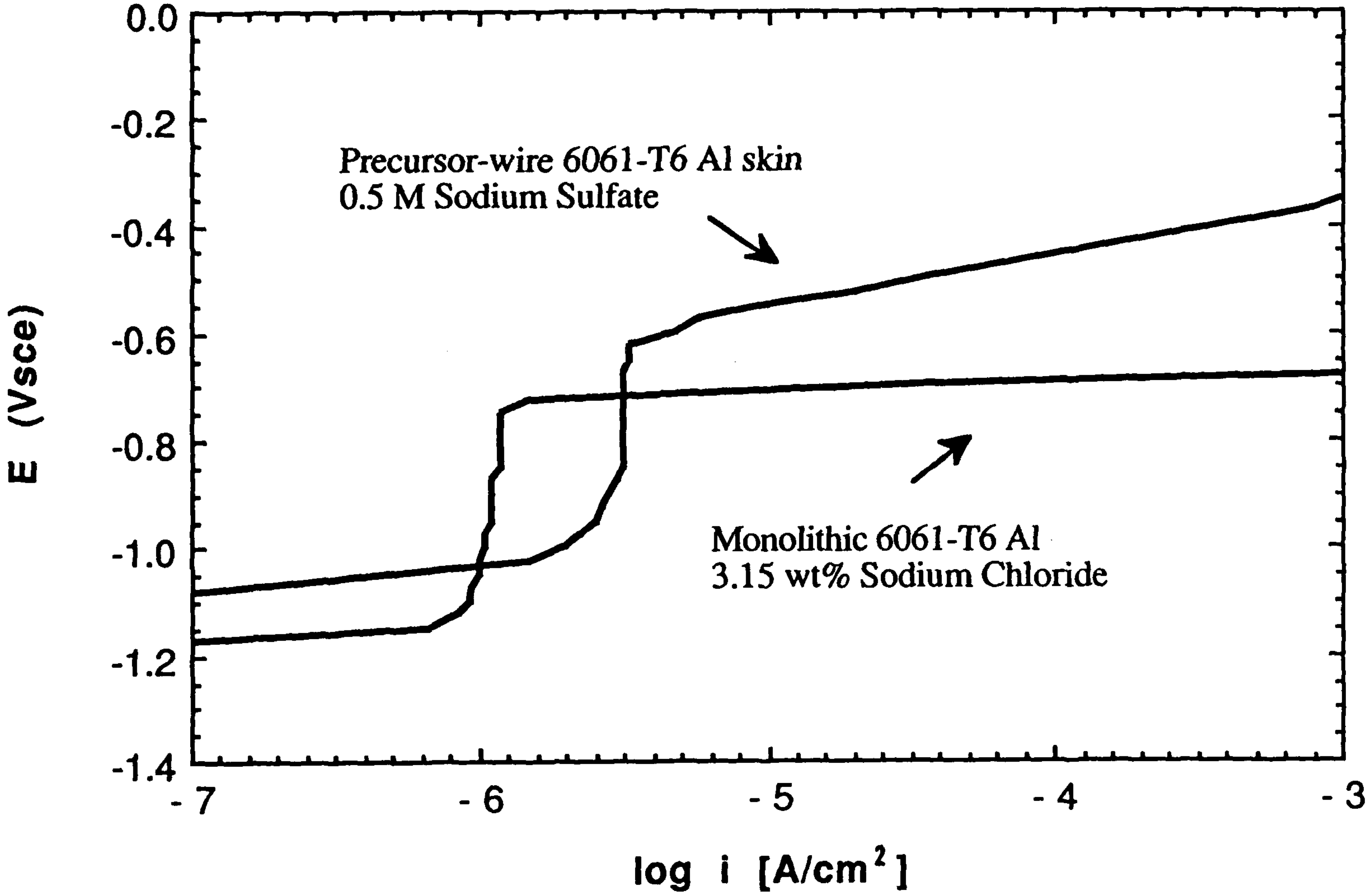

Figure 16: Comparison of the anodic polarization diagram of the precursor-wire 6061-T6 Al skin electrode exposed to deaerated chloride-free 0.5 M Na_2SO_4 to that of monolithic 6061-T6 Al exposed to deaerated 3.15 wt% NaCl. Both solutions were of pH 7 at 30°C. Scan rate = 0.1 mV/s.

BASIC DISTRIBUTION LIST

Technical Reports and Publications — Feb 1990

Organization	Copies
Defense Documentation Center Cameron Station Alexandria, VA 22314	12
Office of Naval Research Dept. of the Navy 800 N. Quincy Street Arlington, VA 22217 ATTN: Code 1131	3
Naval Research Laboratory Washington, DC 20375 ATTN: Codes 6000 6300 2627	 1 1 1
Naval Air Development Center Code 606 Warminster, PA 18974 ATTN: Dr. J. DeLuccia	1
Commanding Officer Naval Surface Warfare Center Silver Spring, MD 20903-5000 ATTN: Library Code R33	 1 1
Naval Ocean Systems Center San Diego, CA 92152-5000 ATTN: Library	1
Naval Postgraduate School Monterey, CA 93940 ATTN: Mechanical Engineering Department	1
Naval Air Systems Command Washington, DC 20360 ATTN: Code 310A Code 5304B Code 931A	 1 1 1
Naval Sea Systems Command Washington, DC 20362 ATTN: Code 05M Code 05R	 1 1
Naval Air Propulsion Center Trenton, NJ 08628 ATTN: Library	1
Naval Civil Engineering Laboratory Port Hueneme, CA 94043 ATTN: Materials Div.	1
Naval Electronics Laboratory San Diego, CA 92152 ATTN: Electronic Materials Sciences Division	1
Commander David Taylor Research Center Bethesda, MD 20084	1
Naval Underwater System Ctr. Newport, RI 02840 ATTN: Library	1
Naval Weapons Center China Lake, CA 93555 ATTN: Library	1
NASA Lewis Research Center 21000 Brookpark Road Cleveland, OH 44135 ATTN: Library	1
National Institute of Standards and Technology Gaithersburg, MD 20899 ATTN: Metallurgy Division Ceramics Division Fracture & Deformation Division	 1 1 1

Naval Facilities Engineering
Command
Alexandria, VA 22331
ATTN: Code 03 1

Commandant of the Marine Corps 1
Scientific Advisor
Washington, DC 20380
ATTN: Code AX 1

Army Research Office
P.O. Box 12211
Research Triangle Park, NC 27709
ATTN: Metallurgy & Ceramics
Program 1

Army Materials Technology Laboratory
Watertown, MA 02172-0001
ATTN: Research Program Office 1

Air Force Office of Scientific
Research
Building 410
Bolling Air Force Base
Washington, DC 20332
ATTN: Electronics & Materials
Science Directorate 1

NASA Headquarters
Washington, DC 20546
ATTN: Code RM 1

Defense Metals & Ceramics
Information Center
Battelle Memorial Inst.
505 King Avenue
Columbus, OH 43201 1

Oak Ridge National Laboratory
Metals and Ceramics Div.
P.O. Box X
Oak Ridge, TN 37380 1
Oak Ridge, TN 37380 1

Los Alamos Scientific Lab.
P.O. Box 1663
Los Alamos, NM 87544
ATTN: Report Librarian 1

Argonne National Laboratory
Metallurgy Division
P.O. Box 229
Lemont, IL 60439 1

Brookhaven National Laboratory
Technical Information Division
Upton, Long Island
New York 11973
ATTN: Research Library 1

Lawrence Berkeley Lab.
1 Cyclotron Rd
Berkeley, CA 94720
ATTN: Library 1

David Taylor Research Ctr
Annapolis, MD 21402-5067
ATTN: Code 281 1
Code 2813 1
Code 0115 1

RE/1131/88/75
4315 (036)

Supplemental Distribution List

Feb 1990

Profs. G.H. Meier and F.S.Pettit
Dept. of Metallurgical and
Materials Eng.
University of Pittsburgh
Pittsburgh, PA 15261

Prof. H.K. Birnbaum
Dept. of Metallurgy & Mining Eng.
University of Illinois
Urbana, Ill 61801

Prof. H.W. Pickering
Dept. of Materials Science and Eng.
The Pennsylvania State University
University Park, PA 16802

Prof. D.J. Duquette
Dept. of Metallurgical Eng.
Rensselaer Polytechnic Inst.
Troy, NY 12181

Prof. D. Tomanek
Michigan State University
Dept. of Physics and Astronomy
East Lansing, MI 48824-1116

Dr. M. W. Kendig
Rockwell International Science Center
1049 Camino Dos Rios
P.O. Box 1085
Thousand Oaks, CA 91360

Prof. R. A. Rapp
Dept. of Metallurgical Eng.
The Ohio State University
116 West 19th Avenue
Columbus, OH 43210-1179

Dr. R. W. Drisko
Code L-52
Naval Civil Engineering Laboratory
Port Hueneme, CA 93043-5003

Dr. R.D. Granata
Zettlemoyer Center for Surface Studies
Sinclair Laboratory, Bld. No. 7
Lehigh University
Bethlehem, PA 18015

Dr. G. D. Davis
Martin Marietta Laboratories
1450 South Rolling Rd.
Baltimore, MD 21227-3898

Prof. P.J. Moran
Dept. of Materials Science & Eng.
The Johns Hopkins University
Baltimore, MD 21218

Prof. J. Kruger
Dept. of Materials Science & Eng.
The Johns Hopkins University
Baltimore, MD 21218

Dr. B.G. Pound
SRI International
333 Ravenswood Ave.
Menlo Park, CA 94025

Prof. C.R. Clayton
Department of Materials Science
& Engineering
State University of New York
Stony Brook
Long Island, NY 11794

Dr. J. W. Oldfield
Cortest Laboratories Ltd
23 Shepherd Street
Sheffield, S3 7BA, England

Prof. Boris D. Cahan
Dept. of Chemistry
Case Western Reserve Univ.
Cleveland, Ohio 44106

Prof. G. Simkovich
Dept. of Materials Science & Eng.
The Pennsylvania State University
University Park, PA 16802

Prof. M.E. Orazem
Dept. of Chemical Engineering
University of Florida
Gainesville, FL 32611